

Supporting Information for

**Modulation of Hydrogel Nanoparticle Intracellular Trafficking by
Multivalent Surface Engineering with Tumor Targeting Peptide**

Leshern Karamchand^{‡a}, Gwangseong Kim^{‡a}, Shouyan Wang^a, Hoe Jin Hah^a, Aniruddha Ray^a,
Ruba Jiddou^a, Yong-Eun Koo Lee^a, Martin A. Philbert^b, and Raoul Kopelman^{*a}

^a Department of Chemistry, University of Michigan, Ann Arbor, Michigan, USA

^b School of Public Health, University of Michigan, Ann Arbor, Michigan, USA

[‡]These authors contributed equally to this work.

*Corresponding author: kopelman@umich.edu

1. Effect of Potassium Depletion on Subcellular Localization of F3 Peptide

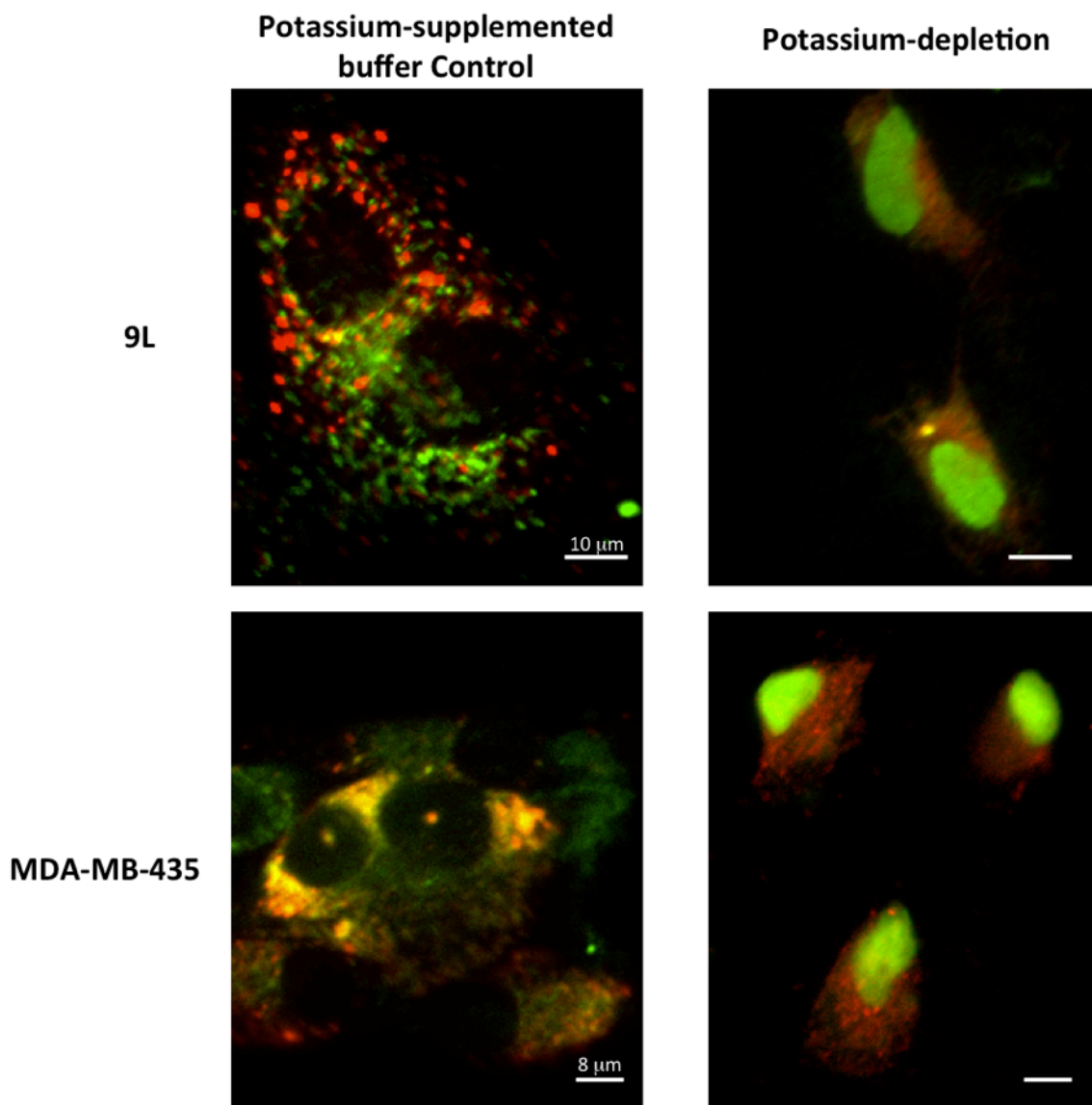
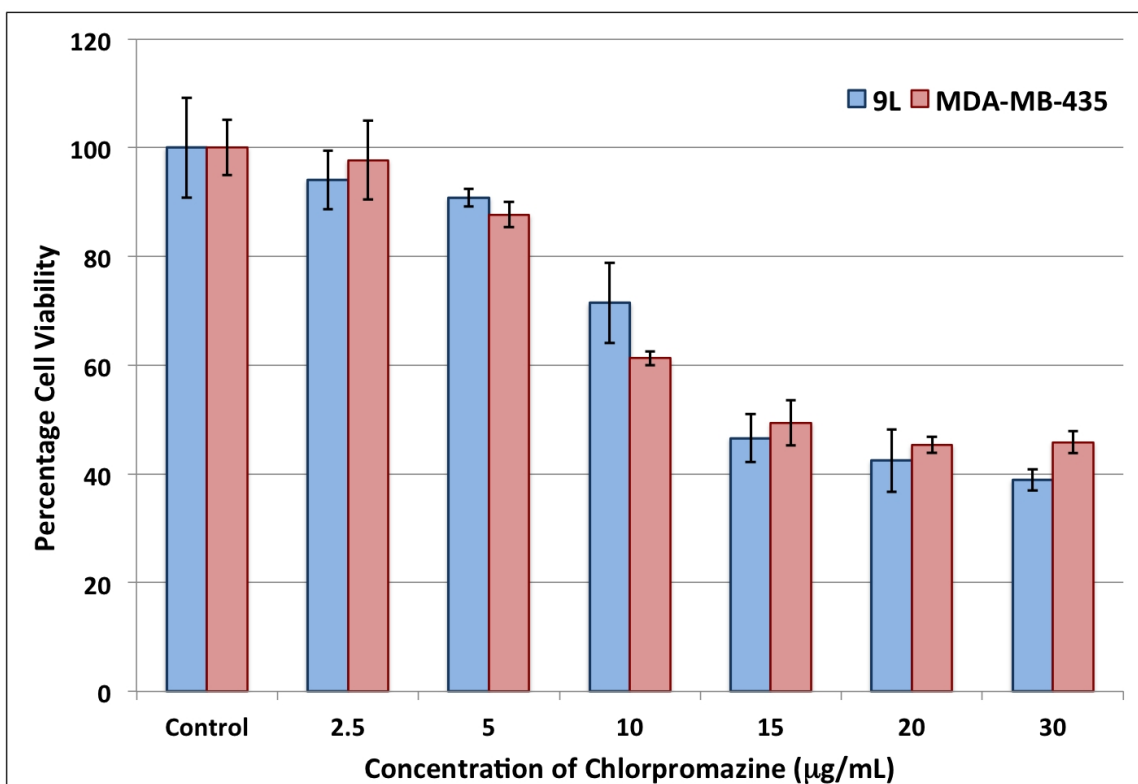
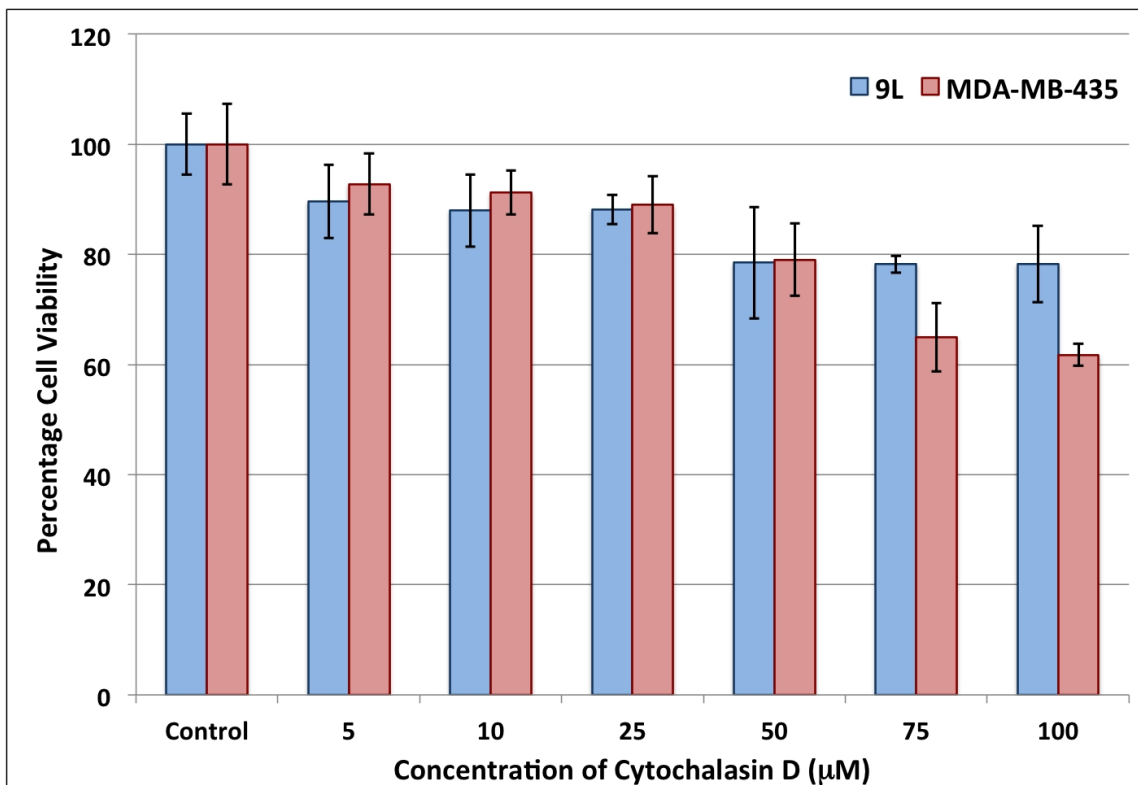


Figure S1. Effect of potassium depletion induced inhibition of clathrin-mediated endocytosis on the subcellular localization of F3 peptide in nucleolin-overexpressing 9L rat gliosarcoma and MDA-MB-435 human melanoma cell lines. As observed for 9L and MDA-MB-435 cells treated with Chlorpromazine, a pharmacological inhibitor of clathrin-mediated endocytosis (Figs. 1.1.c and 2.1.c), potassium-depletion promoted the accumulation of FITC-labeled F3 peptide (green) within the nuclei of both 9L and MDA-MB-435 cells. In the control 9L and MDA-MB-435 cells however, which were treated with potassium-supplemented HEPES buffer, F3 peptide was sequestered either in endosomes, or lysosomes (labeled with Lysotracker Red DND-99) as denoted by regions of yellow fluorescence.

2. Endocytic Inhibitor Cytotoxicity Assays



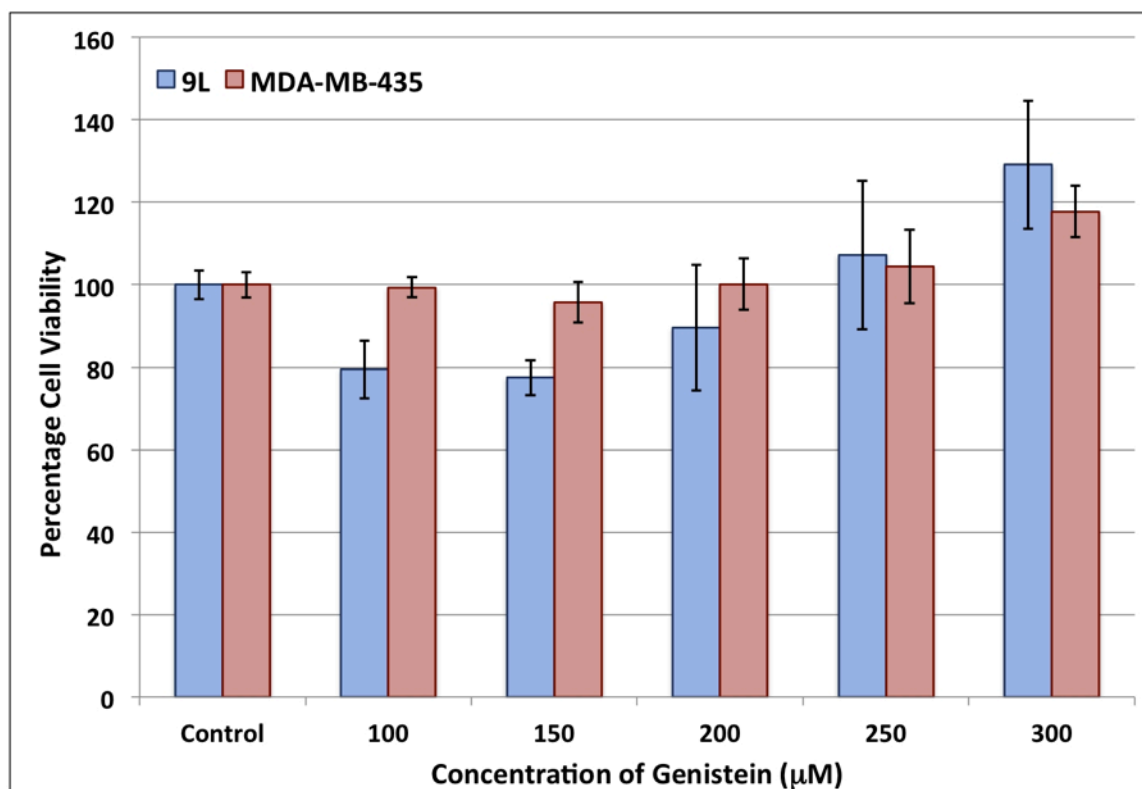


Figure S2.1-2.3. Cytotoxicity profiles of Cytochalasin D (CD), Chlorpromazine (CPZ) and Genistein (GEN), respectively, in the 9L and MDA-MB-435 cell lines, as determined by the Methylthiazol tetrazolium (MTT) microtiter assay. All drug incubations were performed for 90 minutes, at 37 °C, prior to delivery of the MTT reagent to the cells. This inhibitor incubation period was used for all subsequent endocytosis inhibition assays. Maximal concentrations of 50 µM, 10 µg.mL⁻¹, and 200 µM, for CD, CPZ and GEN, respectively, were selected for the endocytosis inhibition assays. In the cases of CD and CPZ, concentrations higher than the abovementioned values were avoided for the endocytosis inhibition assays so as to limit cytotoxicity. Furthermore, concentrations higher than 50 µM CD adversely affected the morphology of both 9L and MDA-MB-435 cells. For GEN, concentrations higher than 200 µM enhanced the viability of both 9L and MDA-MB-435 cells, and were thus avoided, so as to prevent potential stimulation of the F3 peptide or nanoparticle uptake by other endocytic pathways in the presence of GEN. Interestingly, GEN reduced the viability of 9L cells up to 200 µM, but increased their viability, as well as that of the MDA-MB-435 cells, above that of the control cells (107% and 129% for 9L; 104% and 118% for MDA-MB-435) at 250 and 300 µM respectively. A similar trend was reported for GEN in other cell lines.¹ All values are represented as means of quadruplicate wells ± SD.

3. Hydrogel polyacrylamide nanocarrier synthesis and preliminary *in vitro* cell assays

3.1. Size characterization of FITC-labeled hydrogel polyacrylamide nanocarriers

The diameter of the spherical hydrogel PAA-NCs was determined to be 21 ± 5 nm by SEM, which is based on the analysis of 50 individual nanocarrier structures (Fig. S3.1). In aqueous solution, however, the hydrogel PAA-NCs exhibited a median hydrodynamic diameter of approximately 60 nm, as determined by dynamic light scattering (Figs. S3.2 and S3.3). Dynamic light scattering measurements indicated both monodisperse and narrow size distributions for both non-functionalized and F3-targeted, PEGylated PAA-NCs, which confirms that the nanocarriers do not aggregate in solution. This larger size is attributed to the characteristic ability of hydrogels to swell in aqueous solution, and we note that this size may vary with salinity.² Furthermore, the sample preparation procedure for SEM requires dehydration, which indeed causes the hydrogel nanocarriers to shrink and accounts for the discrepancy in size measurements between SEM and DLS methods.

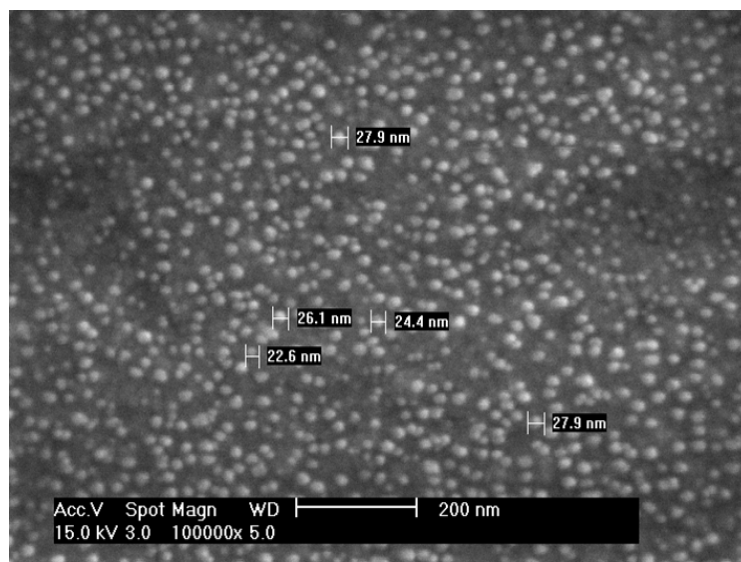


Figure S3.1 Scanning electron micrograph of the polyacrylamide nanocarriers. The nanocarriers exhibited spherical morphology with a mean diameter of 21 ± 5 nm. Magnification: 100,000x.

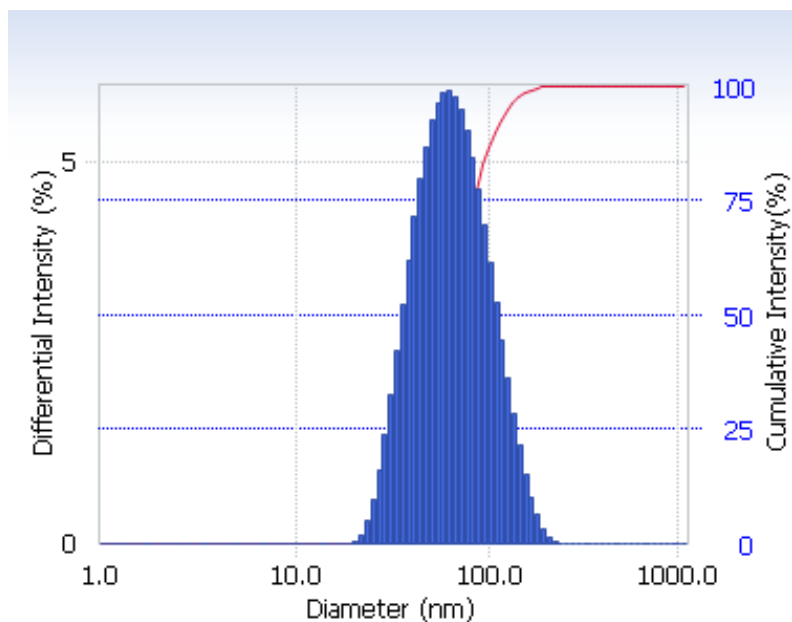


Figure S3.2 Dynamic light scattering data for non-functionalized PAA-NCs (NTNCs) suspended to a final concentration of ($1 \text{ mg}\cdot\text{mL}^{-1}$) in 10 mM PBS buffer. Average diameter: 63.6 nm, Polydispersity index: 0.222

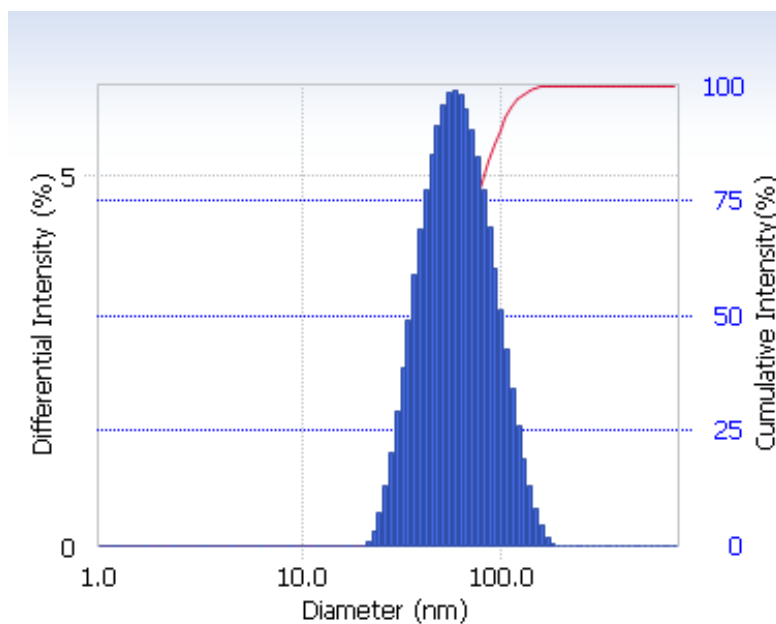


Figure S3.3 Dynamic light scattering data for F3-targeted, PEGylated PAA-NCs (F3NCs) suspended to a final concentration of ($1 \text{ mg}\cdot\text{mL}^{-1}$) in 10 mM PBS buffer. Average diameter: 58.5 nm, Polydispersity index: 0.126

3.2. Optimization of polyacrylamide nanocarrier surface PEGylation

Given the propensity for positively charged nanoparticles to bind non-specifically to the negatively charged cell membranes, we first optimized the PEGylation of the amine surface-functionalized polyacrylamide nanoparticles in order to attenuate their non-specific cell binding, prior to optimizing the surface coverage of these nanoparticles with F3 peptide. Following synthesis, the surfaces of the amine-functionalized FITC-labeled PAA-NCs were modified with heterobifunctional succinimidyl ester-polyethyleneglycol-maleimidyl ester (SCM-PEG-MAL). Briefly, the reaction was achieved in a two-step process; (i) initial conjugation of heterobifunctional PEG molecules via their SCM termini to the primary amine groups on the NC surface, followed by (ii) conjugation of L-cysteine to the MAL termini of the PEG crosslinkers (Cys-capping). The quantity of PEG required to completely neutralize the positive surface charge of amine-functionalized PAA-NCs ($\sim +16$ mV) was determined by reacting increasing amounts of SCM-PEG-MAL (0.4, 2.0 and 4.0 mg) with a fixed mass (50 mg) of PAA-NCs (Fig. S4), followed by measurement of the zeta potential of the resultant PEGylated PAA-NCs. The positive surface charge of the unmodified PAA-NCs is attributed to the presence of protonated amine groups ($-\text{NH}_3^+$) on the NC surface. Figure S4 illustrates the concentration dependent reduction in the positive surface charge of the PAA-NCs by PEG; a ratio of 4 mg PEG: 50 mg lyophilized PAA-NC achieved a reduction in zeta potential from $+16 \pm 2.89$ mV to -0.4 ± 0.82 mV without any observable non-specific binding of these PEGylated PAA-NCs to MDA-MB-435 cells. Figure S4 illustrates the direct correlation between the zeta potential of the non-PEGylated/PEGylated PAA-NCs and their degree of non-specific binding to MDA-MB-435 cells. All subsequent surface PEGylations of the nanocarriers were performed according to the above optimal PEG: PAA-NC ratio.

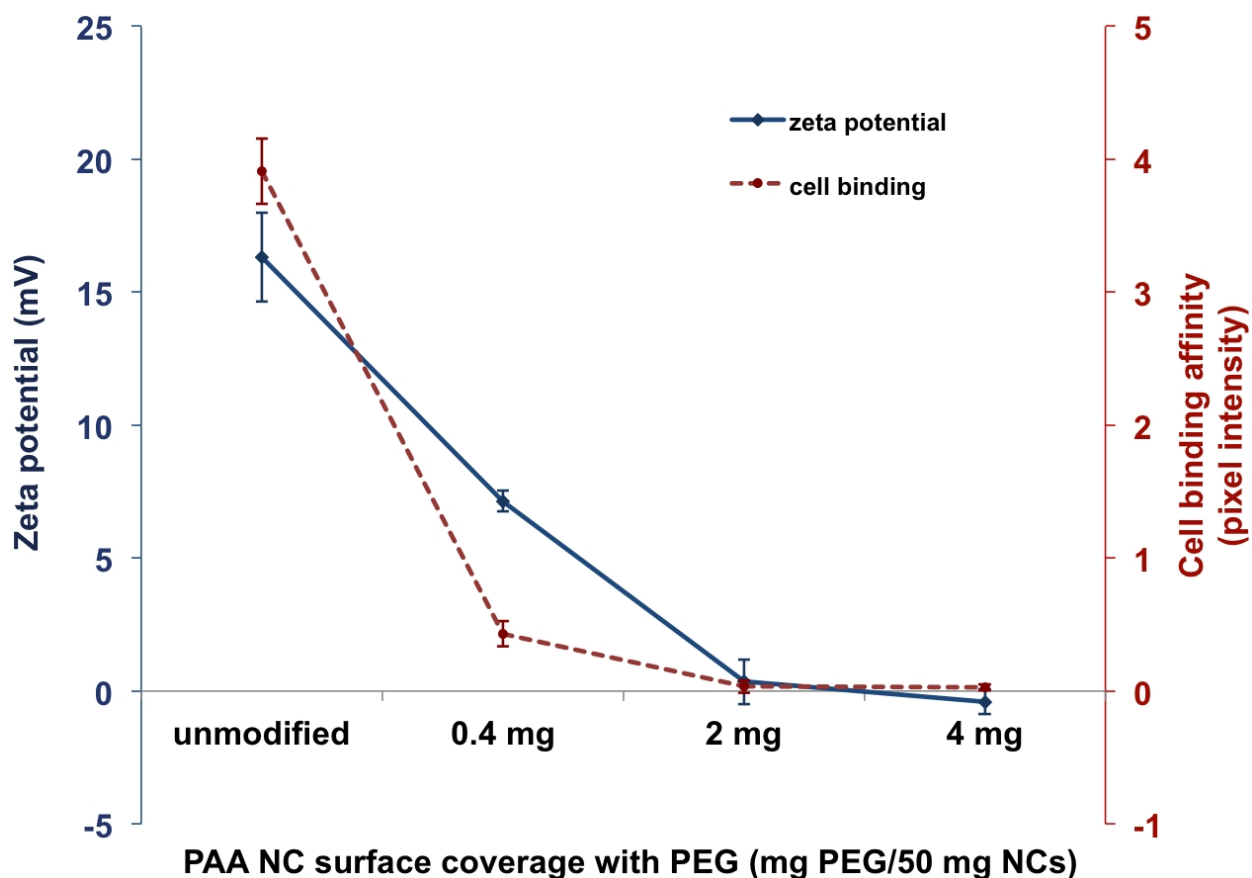


Figure S4. Optimization of PAA nanocarrier surface PEGylation to minimize non-specific cell surface binding. The zeta potential (surface charge) of the various PEGylated PAA nanocarrier formulations was measured by electrophoretic light scattering and compared to their potential for non-specific cell binding to MDA-MB-435 cells. The increase in PAA nanocarrier surface coverage with PEG results in a corresponding decrease in the zeta potential of the PAA nanocarrier, along with a decrease in its potential for non-specific binding to the negatively-charged cell membranes. Since the ratio of 4 mg PEG: 50 mg PAA nanocarriers effectively reduced the zeta potential of the PAA nanocarriers to approximately 0 mV, this formulation was selected for further synthesis of the F3-targeted PEGylated PAA nanocarriers. A reaction ratio of 4 mg PEG to 50 mg PAA-NCs produces a surface coverage of ~40 PEG molecules per single PAA-NC. This was determined by UV/Vis absorption analysis of PAA-NCs functionalized with fluorescein-labeled PEG-succinimidyl ester, as published in a recent study by our lab.³

1.3. Optimization of the F3 peptide surface functionalization

The engineering of the nanoparticle surfaces with multiple targeting ligands (multivalency) has been shown to increase both their cell binding avidity and rate of internalization by the target cells.^{4,5} In addition, the density and availability of cell surface receptors,⁶ as well as the targeting ligand density on the nanocarrier surface,⁷⁻⁹ regulates the internalization of the nanocarrier. This underscores the importance of optimizing the physicochemical properties of a hydrogel nanocarrier, relative to the receptor profile of the target cell and the desired intracellular trafficking pathway, so as to maximize therapeutic efficacy. Given the influence that the degree of ligand coverage on a nanoparticle surface exerts on its cell binding and internalization, we optimized the surface coverage of the PEGylated nanoparticles with F3 peptide, based on their interaction (in terms of cell surface binding and internalization) with the nucleolin-overexpressing 9L and MDA-MB-435 cell lines, prior to studying the intracellular trafficking of the unmodified (non-targeted) PAA-NCs (NTNCs) and F3-targeted (PEGylated) PAA-NCs (F3NCs). Briefly, following surface PEGylation of the PAA-NCs, separate batches of F3NCs, each bearing different degrees of F3 peptide surface coverage, were prepared. Thereafter, each F3NC batch underwent Cys-capping of its PEG crosslinker MAL termini, so as to ensure that the cellular binding of these nanoparticles is governed solely by the interaction between the surface conjugated F3 peptides and the cell surface nucleolin receptors. A linear relationship was observed between the quantity of F3-Cys peptide conjugated to the PEGylated PAA-NC surfaces and the increase in their zeta potential (surface charge) (Fig. S5). This observation is attributed to the multiple arginine and lysine residues of the F3 peptide, whose side-chain amines are positively charged at neutral pH.

Thereafter, the ‘cellular sequestration’ profiles of the nanoparticles (NTNCs and the various F3NC formulations) were determined in two different nucleolin surface-overexpressing live cell lines, MDA-MB-435 human melanoma and 9L rat gliosarcoma, using confocal fluorescence microscopy. The results are summarized in Figure S6.1 and S6.2.

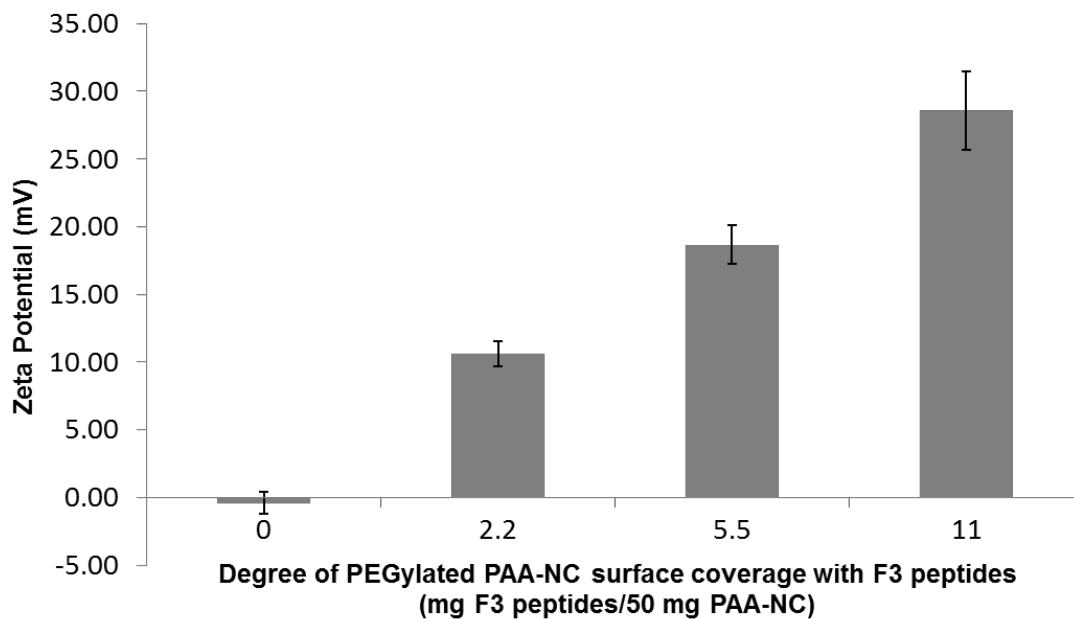


Figure S5. Linear relationship between the degree of surface coverage of the PEGylated PAA-NCs with F3 peptide and their corresponding zeta potentials (surface charge). The average number of F3 peptides per PAA nanocarrier, as determined by Quantitative amino acid analysis (Laboratory for Protein Chemistries, Texas A&M University), is 30 molecules.¹⁰

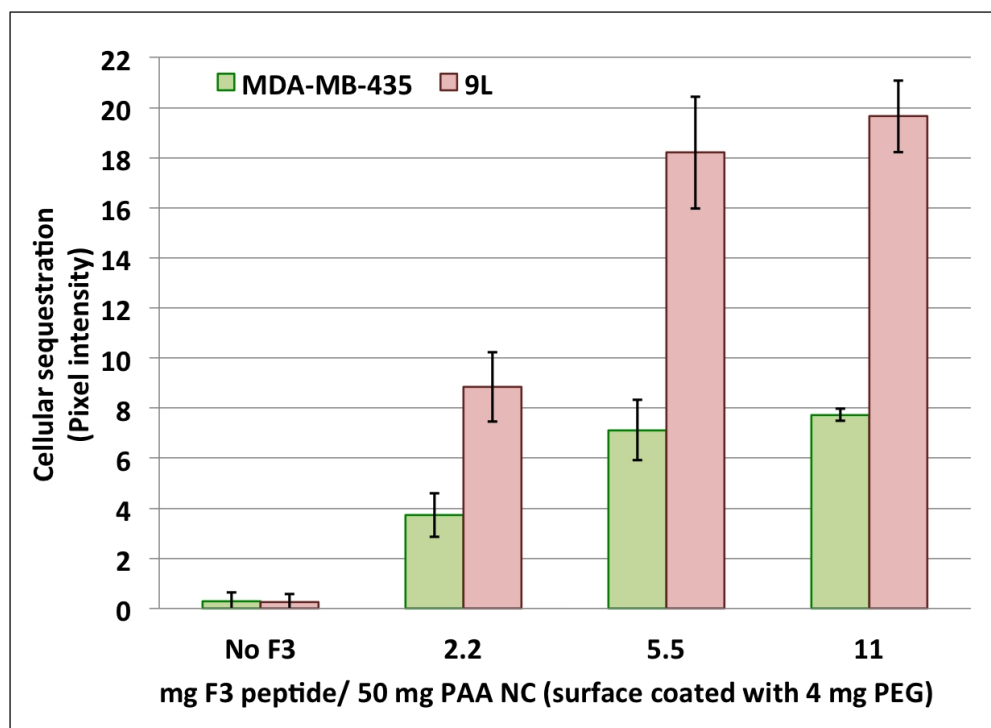


Figure S6.1 Optimization of PEGylated PAA nanocarrier surface functionalization with F3 peptide for optimal cellular sequestration in nucleolin surface-overexpressing cancer cells. Trend of cellular sequestration versus F3 peptide surface coverage of PEGylated PAA nanocarriers in MDA-MB-435 and 9L cell lines. Here, we define the ‘cellular sequestration’ of a nanoparticle as the combination of (i) the degree of nanoparticle-binding to the cell membrane, which is related to the cell binding avidity of that specific nanoparticle, and (ii) the degree to which the nanoparticle is internalized by a particular cell line within a specific period of time. In both the MDA-MB-435 and 9L cell lines, cellular sequestration reached saturation at a ratio of 11 mg F3 peptide: 50 mg PAA-NC.

(S6.2) Table 1: Relative cellular sequestration values for the NTNCs and F3NCs in MDA-MB-435 and 9L cells

F3 surface coverage (mg)	0	2.2	5.5	11
Relative cellular sequestration values				
MDA-MB-435	1.00	13.23	25.34	27.49
9L	1.00	34.60	71.25	76.92

Cellular sequestration values for the F3NCs were normalized relative to that of the unmodified, non-targeted PAA-NCs, for each cell line. The 9L cell line consistently exhibited an approximately 2.7 times higher cellular sequestration for the F3NCs than the MDA-MB-435 cell line.

Experimental Section

Methylthiazol tetrazolium (MTT) Assay of Endocytic Inhibitor Cytotoxicity

Suspensions of 9L and MDA-MB-435 cells, prepared in 10% FBS-supplemented RPMI-1640 and DMEM 11965 media respectively, were seeded into the wells of separate Corning 96-well microtiter plates at approximately 10,000 cells per well, and allowed to attach to the wells for 24 hours at 37 °C in 5% CO₂ humidified atmosphere prior to initiating treatment with the endocytic inhibitors, Cytochalasin D (CD), Chlorpromazine (CPZ) and Genistein (GEN). All inhibitors were prepared in DMSO as 100-fold concentrated stocks, and tested in quadruplicate at the following final concentrations; CD: 5, 10, 25, 50, 75 and 100 μM; CPZ: 2.5, 5, 10, 15, 20 and 30 μg/mL; GEN: 100, 150, 200, 250 and 300 μM. Importantly, all drugs were diluted to the above final concentrations in either RPMI-1640 or DMEM 11965 media such that all dilutions contained equal concentrations of DMSO, which did not exceed 1% v/v. At the start of the assay, all microtiter wells were aspirated of their original culture media and refilled with 200 μL of the appropriate culture medium containing either CD, CPZ or GEN at one of the above concentrations. The vehicle controls constituted 9L and MDA-MB-435 cells treated only with 1% v/v DMSO. The cell lines were then incubated with endocytic inhibitors for 90 min at 37 °C in 5% CO₂ humidified atmosphere. At the end of incubation, all microtiter wells were aspirated of their culture media and replenished with 100 μL of either phenol red-free RPMI-1640 without FBS (for 9L cells) or phenol red-free DMEM culture media without FBS (for MDA-MB-435 cells). Thereafter, 20 μL of 5 mg/mL MTT stock solution (prepared in either phenol red-free RPMI or DMEM media) was added to each well and mixed, followed by further incubation for 4 hours at 37 °C in 5% CO₂ humidified atmosphere. At the end of incubation, the culture media were carefully aspirated from all wells and the purple MTT formazan product in each well was solubilized by addition of 200 μL 100% DMSO solvent, followed by agitation on a rocking shaker overnight at room temperature. Absorbance readings were taken the following day at 550 nm (620 nm reference).

Potassium depletion Assay

Suspensions of 9L and MDA-MB-435 cells, prepared in 10% FBS-supplemented RPMI-1640 and DMEM 11965 media respectively, were seeded into the wells of 8-chambered No. 1 microscopy coverglasses (MatTek Corporation) at approximately 25,000 cells per well and allowed to attach to the coverglasses for 24 hours at 37 °C in 5% CO₂ humidified atmosphere prior to initiating the assay. At the start of the assay, all wells were aspirated of their culture media. Thereafter, the wells containing either 9L or MDA-MB-435 cells designated for potassium depletion were washed once with potassium-depletion buffer (20 mM HEPES, 140 mM NaCl, 1 mM CaCl₂, 1mM MgCl₂, 1 mg/mL D-glucose) and incubated in hypotonic potassium depletion buffer (1:1 ratio of potassium depletion buffer: dH₂O) for 5 minutes at 37 °C. Thereafter, the potassium-depletion wells were washed three times with potassium-depletion buffer, and the cells subsequently incubated with FITC-labeled F3 peptides (0.1 mg/mL) for a further 30 minutes at 37 °C in the same buffer. The control 9L and MDA-MB-435 cells were subjected to the same treatment protocol except with potassium-supplemented buffer (potassium depletion buffer supplemented with 10 mM KCl). At the end of the incubation, all cells were labeled with LysoTracker Red DND-99 (300 nM for 5 minutes at 37 °C). The potassium-depletion and control wells were subsequently washed three times with their respective buffers to remove excess F3 peptides and LysoTracker Red DND-99. The potassium-depletion and control treatments were performed in triplicate for each cell line. The cells were imaged on an Olympus inverted disc-spinning confocal microscope, equipped with an environmental chamber and Semrock BrightLine® Sedat filter set, using a 40x oil-immersion lens. The FITC and TRITC filters were used to excite the FITC-F3 peptides and LysoTracker Red DND-99 fluorophore respectively.

Optimization of PAA-NC Surface PEGylation

Amine-surface functionalized FITC-labeled PAA nanocarriers were synthesized as described in the manuscript. Thereafter, 50 mg lyophilized FITC-labeled PAA-NC was dissolved in 2.5 mL PBS buffer (pH 7.4) and sonicated until the solution turned transparent, to which either 0.4, 2 or 4 mg heterobifunctional PEG crosslinker (SCM-PEG-MAL) was added, and the mixture stirred continuously for 30 min at room temperature. Following washing using an Amicon centrifugal filter (Millipore, 100 kDa molecular weight cut-off), the various PEGylated PAA-NC formulations were reacted with L-cysteine ($62.5 \mu\text{L}$, $10 \text{ mg}\cdot\text{mL}^{-1}$) for 2 hours at room temperature to cap the maleimidyl ester groups of the PEG crosslinkers so as to prevent their reaction with cell surface thiols in subsequent cell-based assays aimed at determining their potential for non-specific cell binding. The PEGylated PAA-NCs were then washed five times with PBS (pH 7.4) using an Amicon centrifugal filter (100 kDa molecular weight cut-off) at $5000 \times g$ for 20 minutes and the various PEGylated PAA-NC formulations resuspended in PBS (pH 7.4) to a final volume of 5 mL. The zeta potentials of the non-PEGylated and various PEGylated PAA-NC formulations were determined as described in the manuscript. Thereafter, the non-PEGylated and various PEGylated PAA-NC formulations were incubated with MDA-MB-435 cells (seeded in 8-chambered multiwell microscopy coverslides; $\sim 100,000$ cells per well) to a final concentration of $0.1 \text{ mg}\cdot\text{mL}^{-1}$ in DMEM supplemented with 10% Fetal Bovine Serum and 1% PSG for 1 hour at 37°C in 5% CO_2 atmosphere. After incubation, the culture media containing unbound non-PEGylated or PEGylated PAA-NCs were aspirated from the wells and the cells washed three times with warm DPBS (pH 7.4). The wells were replenished with colorless DMEM medium and the cells imaged on an Olympus inverted confocal microscope using a 40x objective lens with 488 nm excitation. All images were captured under identical exposure times based on the fluorescence emission of the FITC-labeled PAA-NCs. The degree of non-specific cell binding and internalization of the non-PEGylated and PEGylated PAA-NC formulations was determined by measuring the FITC fluorescence emission intensity from multiple cells

in each confocal plane using Metamorph software (Molecular Devices). All values are reported as means from three independent experiments.

Optimization of Surface Functionalization of PEGylated PAA-NCs with F3 peptide

Fresh batches of PEGylated PAA-NCs (4 mg SCM-PEG-MAL: 50 mg FITC-PAA-NCs) were prepared as described above, however with omission of the Cys-capping stepping of the MAL groups on the PEG crosslinkers. After washing to remove unbound PEG crosslinkers, separate batches of surface PEGylated PAA-NCs were reacted with different quantities of F3-Cys (2.2, 5.5 or 11 mg), and the conjugation reaction allowed to run overnight at room temperature. The reaction between the thiol group of the carboxy terminal cysteine of the F3 peptide moieties and the maleimidyl ester termini of the PEG crosslinkers facilitated covalent conjugation of the F3 peptide moieties to the PEG crosslinkers already conjugated to the PAA-NC surfaces. The F3 surface functionalized PEGylated PAA-NCs (F3NCs) were subsequently incubated with 1.74 mg of L-cysteine for 2 hours at room temperature to cap any unreacted maleimidyl ester groups. Thereafter, the different F3NC batches were washed five times with PBS (pH 7.4) using an Amicon centrifugal filter (100 kDa molecular weight cut-off) at 4000 xg for 20 minutes and the final volume adjusted to 5 mL with PBS (pH 7.4). The zeta potentials of the various F3NC formulations were determined as described in the manuscript. The filtered nanocarriers were kept frozen at -20 °C until use.

Live cell assays: MDA-MB-435 and 9L cell lines were seeded in separate 8-chambered multiwell microscopy coverslides (~ 140, 000 cells per well) in their respective complete culture media, and incubated overnight at 37 °C in a 5% CO₂ humidified atmosphere. The following day, the cells were treated with the various F3NC formulations, at a final concentration of 0.1 mg.mL⁻¹ for 1 hour at 37 °C. Thereafter, any unbound F3NCs were rinsed away by three changes of culture medium. The wells were replenished with colorless culture media, and confocal imaging of the F3NC-treated cell lines was

performed directly from the multi-well coverslides on an Olympus inverted confocal microscope, using a 40x objective lens with 488 nm excitation. Images were captured under identical exposure times, based on the fluorescence emission of the FITC-labeled F3NCs. The F3NC cellular sequestrations were quantified by measuring the pixel intensity of each cell from the obtained confocal images, using Metamorph software (Molecular Devices). All values are reported as means from three independent experiments.

References

1. D. Vercauteren, R. E. Vandenbroucke, A. T. Jones, J. Rejman, J. Demeester, S. C. De Smedt, N. N. Sanders, and K. Braeckmans, *Molecular Therapy*, 2010, **18**, 561-569.
2. H. H. Hooper, J. P. Baker, H. W. Blanch, and J. M. Prausnitz, *Macromolecules*, 1990, **23**, 1096–1104.
3. N. Guochao, H. J. Hah, G. Kim, Y-E Koo Lee, M. Qin, T. S. Ratani, P. Fotiadis, A. Miller, A. Kochi, D. Gao, T. Chen, D. A. Orringer, O. Sagher, M.A. Philbert and R. Kopelman, *Small*, 2012, 1-8
4. F. Gu, L. Zhang, B. a Teply, N. Mann, A. Wang, A. F. Radovic-Moreno, R. Langer, and O. C. Farokhzad, *Proceedings of the National Academy of Sciences of the United States of America*, 2008, **105**, 2586–91.
5. D. R. Elias, A. Poloukhine, V. Popik, and A. Tsourkas, *Nanomedicine : nanotechnology, biology, and medicine*, 2012, 1–8.
6. E. Ruoslahti, S. N. Bhatia, and M. J. Sailor, *The Journal of cell biology*, 2010, **188**, 759–68.
7. H. Yuan and S. Zhang, *Applied Physics Letters*, 2010, **96**, 033704.
8. H. Yuan, C. Huang, and S. Zhang, *PloS one*, 2010, **5**, e13495.
9. A. Fakhari, A. Baoum, T. J. Siahaan, K. B. Le, and C. Berkland, *Journal of pharmaceutical sciences*, 2011, **100**, 1045–56.
10. G, R, Reddy, M. S. Bhojani, P. McConville, J. Moody, B. A. Moffat, D. E. Hall, G. Kim, Y-E. L. Koo, M. J. Woolliscroft, J. V. Sugai, T. D. Johnson, M. A. Philbert, R. Kopelman, A. Rehemtulla and B. D. Ross, *Clinical Cancer Research*, 2006, **12**, 6677-6686.